Electronic structure and x-ray magnetic circular dichroism in uranium compounds. I. UFe_2

V. N. Antonov* and B. N. Harmon
Ames Laboratory, Iowa State University, Ames, Iowa 50011, USA

A. N. Yaresko
Max Planck Institute for Physics of Complex Systems, D-01187 Dresden, Germany
(Received 10 September 2003; published 24 December 2003)

The electronic structure, magneto-optical and x-ray magnetic circular dichroism (XMCD) spectra of UFe_2 were investigated theoretically from first principles, using the fully relativistic Dirac linear muffin-tin orbital band-structure method. The electronic structure is obtained with the local spin-density approximation (LSDA), as well as with a generalization of the LSDA+U method which takes into account the nondiagonal occupation matrix (in spin indexes) of localized electrons. The origin of the Kerr rotation and XMCD spectra in the compound is examined.

DOI: 10.1103/PhysRevB.68.214424 PACS number(s): 75.30.Mb, 71.28.+d

I. INTRODUCTION

Uranium compounds exhibit a rich variety of properties to a large extent because of the complex behavior of their $5f$ electrons. The $5f$ states in U are intermediate between the itinerant $3d$ electrons in transition metals and the localized $4f$ electrons in rare-earth compounds. The determination of the electronic structure of U compounds is a challenging task because in many of them the width of the $5f$ bands, their spin-orbit splitting, and the on-site Coulomb repulsion in the partially filled $5f$ shell are of the same order of magnitude and should be taken into account on the same footing. Interest in uranium compounds has recently been renewed, especially after the discovery of such unusual effects as heavy fermion superconductivity and the coexistence of superconductivity and magnetism.

UFe_2 is one of the actinide compounds that has been intensively studied for several decades.[1–6] Below 160 K UFe_2 is a ferromagnet with a low magnetic anisotropy similar to that of pure iron. Interest in this compound arises from the fact that the total moment on the uranium site is very small as was first deduced from neutron-diffraction experiments.[7,8] Evidence for strong hybridization between the U $5f$ and Fe $3d$ electrons in UFe_2 was first theoretically provided by spin-polarized band-structure calculations performed by Brooks *et al.* in Ref. 9. They predicted that one consequence of the hybridization would be a reduction, as compared to the free-ion value in the orbital moment of uranium. Using polarized neutrons and elastic scattering Wulff *et al.*[10] and Lebech *et al.*[11] showed that this was, in fact, the case. The orbital and spin moments are both of about $0.25\mu_B$, but they are oppositely directed, and hence the net moment, which is the sum of the orbital and spin contributions, on the U site is close to zero. The neutron experiments[10,11] on single crystals of UFe_2 also showed that the Fe moment is $(0.60\pm0.03)\mu_B$, a substantial reduction from the $2.2\mu_B$ of pure Fe. Recently[12] the spin and orbital moments on the uranium site in UFe_2 have been deduced from x-ray magnetic circular dichroism (XMCD) data by using sum rules. It was found that $M_L = 0.21\mu_B$ and $M_S = -0.20\mu_B$ in agreement with the results given by polarized neutron scattering.[11] Spin moments were also derived from the magnetic-Compton profile of UFe_2 in Ref. 13, and found to be equal to $-0.20\mu_B$ and $0.52\mu_B$ at U and Fe sites, respectively. UFe_2 was also studied by means of photoelectron spectroscopy which showed a pronounced structure at the Fermi level that extends some 2–3 eV below E_F and originates from U $5f$ states.[14,15]

In order to examine how the hybridization between $5f$ electrons of uranium and the $3d$ electrons of iron affects the magnetic exchange parameters and spin-wave spectra, measurements of spin dynamics in UFe_2 were performed in Refs. 16,17. There are two important results emerging from these measurements. The first is the large Fe-Fe exchange parameter $J_{\text{Fe-Fe}}$ (or equivalently the large spin-wave stiffness constant) deduced from the Fe spin-wave model. It is actually unprecedented that diluting Fe results in a larger Fe-Fe exchange. The increase in $J_{\text{Fe-Fe}}$ must surely come from the $5f$-$3d$ interaction. The second point is the absence of any scattering involving the uranium spins. The absence of, in particular, the acoustic U mode was attributed to the tendency of magnetic response of the $5f$ states to spread over $(\omega,\mathbf{q})$ space because of hybridization with the $3d$ electrons of iron.[16]

Paolasini *et al.*[18] measured the phonon-dispersion curves in YFe_2, UFe_2, and $CeFe_2$ Laves phases by inelastic neutron scattering. The phonon-dispersion curves and the generalized phonon densities of states were evaluated by a Born–von Karman model. Many differences in the phonon spectrum are found in UFe_2 with respect to the isostructural $REFe_2$ compounds (RE=rare earth). Compared to the expectation based on the knowledge of other $REFe_2$ compounds, the Fe-Fe and U–Fe longitudinal force constants exhibit a large increase in UFe_2, whereas the U-U longitudinal force constants are substantially reduced. Furthermore, the Fe-Fe transverse force constants in UFe_2 are negative, whereas these parameters are usually near to positive and small in the Laves phases.[18] Normally a negative force constant indicates an incipient structural instability, but this is prevented by other interactions. It is tempting to ascribe these dramatic changes in the UFe_2 force constants, compared to those of the other materials, to electronic interactions. Such interac-

tions, arising presumably from the hybridization of U $5f$ and Fe $3d$ itinerant electrons, may also be responsible for the large magnetoelastic interactions found in UFe_2.[3]

The experimental measurements of the magneto-optical (MO) properties of UFe_2 were recently reported by Kucera *et al.*[19] Oppeneer *et al.* calculated the MO spectra of UFe_2 in the local spin-density approximation (LSDA).[20] The experimentally measured spectra appeared later, therefore their calculations can be considered as a prediction. The calculations have been made for both the (001) and (111) directions of magnetic field, and quite small magnetocrystalline anisotropy in the Kerr spectrum of UFe_2 were obtained. This might be related to the cubic crystal symmetry and, possibly, also to the small U moment.[20] The calculations included only interband transitions, as a result, a deep minimum in the Kerr rotation spectrum in the 0 to 1.5 eV energy range was obtained, which is not observed in the experimental spectrum.[19]

The x-ray magnetic circular dichroism technique developed in recent years has evolved into a powerful magnetometry tool to separate orbital and spin contributions to element specific magnetic moments. X-ray magnetic circular dichroism experiments consist of measuring the absorption of x rays with opposite (left and right) states of circular polarization. Study of the $5f$ electron shell in uranium compounds is usually performed by tuning the energy of the x ray close to the $M_{4,5}$ edges of uranium (located at 3552 and 3728 eV, respectively) where electronic dipole transitions between $3d_{3/2,5/2}$ and $5f_{5/2,7/2}$ states occur. Recently XMCD measurements have been successfully performed for uranium compounds such as US,[21,22] $USb_{0.5}Te_{0.5}$,[23] $U_xLa_{1-x}S$,[24] UBe_{13} and UPt_3,[25] UFe_2,[12,26] UNi_2Al_3,[27] UPd_2Al_3 and URu_2Si_2,[28] URhAl,[29] UCoAl and UPtAl.[30] There are some features in common for all the uranium compounds investigated up to now. First, the dichroism at the M_4 edge is much larger, sometimes one order of magnitude larger, than at the M_5 one. Second, the dichroism at the M_4 edge has a single negative lobe that has no distinct structure, on the other hand, two lobes, a positive and a negative one, are observed at the M_5 edge. Concerning the line shape of the XMCD signal, the investigated metallic uranium compounds fall into two types according to the relative intensity of the positive and negative lobes observed at the M_5 edge. The two lobes have almost equal intensity for UP_3, UPd_2Al_3, UPtAl, and UBe_{13}. On the other hand, the positive lobe is smaller in comparison with the negative one for US, $USb_{0.5}Te_{0.5}$, UFe_2, URu_2Si_2, UCoAl, and URhAl.

With the above as background, we have performed calculations to evaluate the XMCD properties for a number of uranium ferromagnetic materials. Besides the inherent interest in the materials studied, the use of similar methods to study materials with different degrees of localized U $5f$ electronic states helps to establish the limitations of the LSDA approach and to identify where techniques like the LSDA $+U$ method are needed. We have divided the work into three papers, with this paper I, concentrating on the description of the methods and the results for the UFe_2. This compound, as widely believed, belongs to the class of uranium compounds with itinerant $5f$ electrons. Paper II deals with UTAl (T = Co, Rh, or Pt) intermetallics. Paper III is devoted to the electronic structure and XMCD spectra of some heavy-fermion uranium compounds UPt_3, URu_2Si_2, UPd_2Al_3, UNi_2Al_3, and UBe_{13}. We use both the LSDA and LSDA $+U$ approaches to assess the sensitivity of the XMCD results to different treatments of the correlated electrons.

The comparison between experiment and theory provides insight into the nature of the $5f$ electrons and offers some evaluation of the suitability of several electronic structure methods for treating $5f$ electrons. In a few cases it is clear that more sophisticated many-body approaches are needed if satisfactory quantitative agreement is to be achieved.

This paper is organized as follows. Section II presents a description of the crystal structure of UFe_2 and the computational details. Section III is devoted to the electronic structure, MO and XMCD properties of UFe_2 calculated in the LSDA and LSDA$+U$ approximations. The MO and XMCD theoretical calculations are compared to the experimental measurements. Finally, the results are summarized in Sec. IV.

II. CRYSTAL STRUCTURE AND COMPUTATIONAL DETAILS

UFe_2 crystallizes in the cubic face-centered O_h^7 Laves phase ($Fd3m$ space group) with eight formula units per unit cell. Six atoms are required to specify the primitive cell, which contains only two inequivalent sites: four Fe atoms ($16d$ positions) form a tetrahedral sublattice whereas two U atoms ($8a$ positions) form the characteristic diamond sublattice. The nearest Fe-Fe distance in this structure ($\sim$2.5 Å with coordination number 6) is actually shorter than found in pure iron (2.8 Å with coordination number 8). The U-U separation in UFe_2 is also rather small (3.05 Å).

We now turn to a description of the magneto-optical effects, which refer to various changes in the polarization state of light upon interaction with materials possessing a net magnetic moment, including rotation of the plane of linearly polarized light (Faraday, Kerr rotation), and the complementary differential absorption of left and right circularly polarized light (circular dichroism). In the near visible spectral range these effects result from excitation of electrons in the conduction band. Near x-ray-absorption edges, or resonances, magneto-optical effects can be enhanced by transitions from well-defined atomic core levels to valence states selected by transition matrix element symmetry. There are at least two alternative formalisms for describing resonant x-ray MO properties. One approach uses the classical dielectric tensor.[31] Another one uses the resonant atomic scattering factor including charge and magnetic contributions.[32,33] The equivalence of these two description (within the dipole approximation) is demonstrated in Ref. 34.

For the polar Kerr magnetization geometry and a crystal of tetragonal symmetry, where both the fourfold axis and the magnetization **M** are perpendicular to the sample surface and the z axis is chosen to be parallel to them, the dielectric tensor is composed of the diagonal ε_{xx} and ε_{zz}, and the off-diagonal ε_{xy} components and has the form

$$\varepsilon = \begin{pmatrix} \varepsilon_{xx} & \varepsilon_{xy} & 0 \\ -\varepsilon_{xy} & \varepsilon_{xx} & 0 \\ 0 & 0 & \varepsilon_{zz} \end{pmatrix}. \quad (1)$$

In the polar geometry the expression for the complex Kerr angle can be easily obtained for small angles and is given by[35]

$$\theta_K(\omega) + i\varepsilon_K(\omega) = -\sigma_{xy}(\omega)/D(\omega), \quad (2)$$

where

$$D(\omega) = \sigma_{xx}(\omega)\sqrt{1 + \frac{4\pi i}{\omega}\sigma_{xx}(\omega)}, \quad (3)$$

with θ_K being the Kerr rotation and ε_K being the so-called Kerr ellipticity. $\sigma_{\alpha\beta}$ $(\alpha,\beta \equiv x,y,z)$ is the optical conductivity tensor, which is related to the dielectric tensor $\varepsilon_{\alpha\beta}$ through

$$\varepsilon_{\alpha\beta}(\omega) = \delta_{\alpha\beta} + \frac{4\pi i}{\omega}\sigma_{\alpha\beta}(\omega). \quad (4)$$

Using straightforward symmetry considerations it can be shown that all magneto-optical phenomena (XMCD, MO Kerr, and Faraday effects) are caused by the symmetry reduction, in comparison to the paramagnetic state, caused by magnetic ordering.[36] This symmetry lowering has consequences only when spin-orbit (SO) coupling is considered in addition. Therefore, in order to calculate the XMCD properties one has to account for both magnetism and SO coupling at the same time when dealing with the electronic structure of the material considered. Theoretical descriptions of magnetic dichroism can be cast into four categories. On one hand, there are one-particle (ground-state) and many-body (excited-state) theories; on the other hand, there are theories for single atoms and those which take into account the solid state. To name a few from each category, for atomic one-particle theories we refer to Refs. 37 and 38, for atomic many-particle multiplet theory to Refs. 39–42, for many-particle theories for solids to Ref. 43, and for one-particle theories (photoelectron diffraction) for solids to Refs. 44–47. A multiple-scattering approach to XMCD, a solid-state one-particle theory, has been proposed by Ebert *et al.*[48–50] and Tamura *et al.*[51]

Within the one-particle approximation, the absorption coefficient μ for incident x rays of polarization λ and photon energy $\hbar\omega$ can be determined as the probability of electron transitions from an initial core state (with wave function ψ_j and energy E_j) to a final unoccupied state (with wave functions $\psi_{n\mathbf{k}}$ and energy $E_{n\mathbf{k}}$)

$$\mu_j^{\lambda}(\omega) = \sum_{n\mathbf{k}} |\langle \Psi_{n\mathbf{k}} | \mathcal{J}_{\lambda} | \Psi_j \rangle|^2 \delta(E_{n\mathbf{k}} - E_j - \hbar\omega)\,\theta(E_{n\mathbf{k}} - E_F), \quad (5)$$

with $\mathcal{J}_{\lambda} = -e\boldsymbol{\alpha}\mathbf{a}_{\lambda}$ being the dipole electron-photon interaction operator, where $\boldsymbol{\alpha}$ are Dirac matrices, $\mathbf{a}_{\lambda}$ is the λ polarization unit vector of the photon vector potential $[a_{\pm} = 1/\sqrt{2}(1,\pm i,0), a_z = (0,0,1)]$. (Here $+/-$ denotes, respectively, left and right circular photon polarizations with respect to the magnetization direction in the solid).

While the XMCD spectrum is calculated using Eq. (5), some of its features can be understood already from a simplified expression for paramagnetic solids. By restricting oneself to electric dipole transitions, performing the integration only inside atomic spheres (due to the highly localized core sates), and averaging with respect to the polarization of the light, one obtains the following expression for the absorption coefficient of the core level with (l,j) quantum numbers,[52]

$$\mu_{lj}^0(\omega) = \sum_{l',j'} \frac{2j+1}{4}\left(\frac{\delta_{l',l+1}\delta_{j',j+1}}{j+1} + \frac{\delta_{l',l-1}\delta_{j',j-1}}{j} + \frac{\delta_{l',l+1}\delta_{j',j}}{j(j+1)(2j+1)} \right) N_{l',j'}(E) C_{l,j}^{l',j'}(E), \quad (6)$$

where $N_{l',j'}(E)$ is the partial density of the empty states and $C_{l,j}^{l',j'}(E)$ the radial matrix elements.[52]

In order to simplify the comparison of the theoretical x-ray isotropic absorption $M_{4,5}$ spectra of UFe_2 to the experimental ones we take into account the background intensity which affects the high-energy part of the spectra. The shape of x-ray absorption caused by the transitions from inner levels to the continuum of unoccupied levels was first discussed by Richtmyer *et al.* in the early thirties.[53] The absorption coefficient with the assumption of equally distributed empty continuum levels is

$$\mu(\omega) = \frac{C\Gamma_c}{2\pi}\int_{E_{cf_0}}^{\infty} \frac{dE_{cf}}{(\Gamma_c/2)^2 + (\hbar\omega - E_{cf})^2}, \quad (7)$$

where $E_{cf} = E_c - E_f$, E_c, and Γ_c are the energy and the width of a core level, E_f is the energy of empty continuum levels, E_{f_0} is the energy of the lowest continuum level, and C is a normalization constant which has been used as an adjustable parameter.

The intrinsic broadening mechanisms were also accounted for by folding XMCD spectra with Lorentzians of half-width of 3.4 and 3.7 eV for the M_5 and M_4 spectra, respectively.

The details of the computational method are described in our previous papers,[54,55] and here we only mention several aspects. The calculations were performed for the experimentally observed lattice constant $a = 7.055$ Å using the LMTO method[56,57] in the atomic sphere approximation with the combined correction term taken into account. The radii of atomic spheres for U and Fe were chosen to be equal to 3.2250 and 2.6414 a.u., respectively. We used the von Barth–Hedin parametrization[58] for the exchange-correlation potential. Brillouin zone integrations were performed using the improved tetrahedron method[59] and charge self-consistency was obtained with 349 irreducible **k** points. The basis consisted of U *s*, *p*, *d*, *f*, and *g*; Fe *s*, *p*, *d*, and *f* LMTO's. The combined correction terms were also included in calculation of the optical matrix elements.[60] We calculated the absorptive part of the optical conductivity in a wide energy range

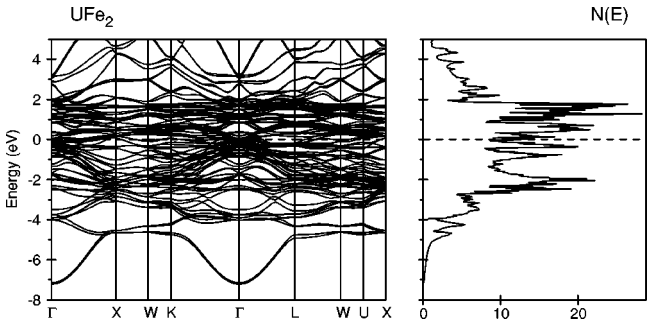

FIG. 1. The LSDA self-consistent fully relativistic, spin-polarized energy-band structure and total DOS [in states/(unit cell eV)] of UFe_2.

and then the Kramers-Kronig transformation was used to calculate the dispersive parts of the optical conductivity from the absorptive parts.

We have adopted the LSDA+U method[61,62] as a different level of approximation to treat the electron-electron correlation. We used a generalization of the LSDA+U method which takes into account spin-orbit coupling so that the occupation matrix of localized electrons becomes nondiagonal in spin indexes. This method is described in detail in our previous paper[62] including the procedure to calculate the screened Coulomb U and exchange J integrals, as well as the Slater integrals F^2, F^4, and F^6.

III. RESULTS AND DISCUSSION

A. Band structure and magnetic moments

The fully relativistic spin-polarized LSDA energy-band structure and total density of states (DOS) of the ferromagnetic UFe_2 compound are shown in Fig. 1. The bands in the lowest region between -7.3 and -4.0 eV have mostly Fe s character with a small amount of U spd character mixed in. The energy bands between -4.0 and -0.3 eV are predominantly Fe $3d$ states. The U $5f$ energy bands are located in the vicinity of E_F in the energy range -0.4 to 2.0 eV. There is a strong hybridization between the U $5f$, $6d$, and Fe $3d$ states.

In magnets, the atomic spin M_s and orbital M_l magnetic moments are basic quantities and their separate determination is therefore important. Methods of their experimental determination include traditional gyromagnetic ratio measurements,[63] magnetic form-factor measurements using the neutron scattering,[64] and magnetic x-ray scattering.[65] In addition to these, the recently developed x-ray magnetic circular dichroism combined with several sum rules[66,67] has attracted much attention as a method of site- and symmetry-selective determination of M_s and M_l. Table I presents the comparison between calculated and experimental magnetic moments in UFe_2. Polarized neutrons and elastic scattering[10,11] as well as x-ray magnetic circular dichroism measurements[12] reveal that the orbital and spin magnetic moments on the U site are almost equal and oppositely directed, hence the U net moment, which is the sum of the orbital and spin contributions, is close to zero in UFe_2. The LSDA calculations do not provide such a compensation (Table I). The LSDA total magnetic moment of uranium in UFe_2 is equal to $-0.26\mu_B$ (Table I) (with spin moment $-0.61\mu_B$ and orbital moment $0.35\mu_B$). The calculated uranium moment is dominated by $5f$ states: the $5f$ components of the spin and orbital moment are $-0.50\mu_B$ and $0.34\mu_B$, respectively.

It is a well-known fact, however, that the LSDA calculations fail to produce the correct value of the orbital moment of uranium compounds.[68–72] In the LSDA, the Kohn-Sham equation is described by a local potential which depends on the electron spin density. The orbital current, which is responsible for M_l, is, however, not included into the equations. This means, that although M_s is self-consistently determined in the LSDA, there is no framework to determine simultaneously M_l self-consistently.

Numerous attempts have been made to better estimate M_l in solids. They can be roughly classified into two categories. One is based on the so-called current density-functional theory[73–75] which is intended to extend density-functional theory to include the orbital current as an extra degree of freedom, which describes M_l. Unfortunately an explicit form of the current density functional is at present unknown. The other category includes orbital polarization (OP),[69–72] self-interaction correction,[76] and LSDA+U[77,62] approaches, which provide a means to calculate M_l beyond the LSDA scheme.

For a better description of M_l, the OP functional form of BL_z^2 with the Racah parameter B has been deduced[69] from an atomic multiplet ground state without spin-orbit interaction

TABLE I. The experimental and calculated spin M_s, orbital M_l, and total M_t magnetic moments (in μ_B) of UFe_2.

	U			Fe			UFe_2
	M_s	M_l	M_t	M_s	M_l	M_t	M_t
LSDA	−0.61	0.35	−0.26	0.68	0.06	0.74	1.22
LSDA+U(OP)	−0.71	0.72	0.01	0.71	0.08	0.79	1.59
LSDA+U	−1.83	3.08	1.25	1.14	0.20	1.34	2.59
LSDA (Ref. 70)	−0.71	0.47	−0.24	0.75	0.07	0.82	1.40
LSDA+OP (Ref. 70)	−1.03	0.88	−0.15	0.82	0.07	0.89	1.63
expt.[11]	−0.22	0.23	0.01	0.59			1.19
expt.[12]	−0.20	0.21	0.01				
expt.[13]	−0.20			0.52			

(SOI), where S and L are given by Hund's rules. However, the OP method does not assure us that it will give a good description when the SOI is included and thus S and L are no longer good quantum numbers. The inclusion of the OP correction in Ref. 70 brings the calculated total U moment in UFe_2 to $-0.15\mu_B$, in better agreement with experiment compared to the LSDA calculations (Table I).

Solovyev *et al.*[77] argued that the key parameter responsible for the exchange-correlation enhancement of the orbital magnetic moments in solids is the "Hubbard U" rather than the intra-atomic Hund's second rule coupling, being consistent with a more general concept of the orbital polarization. This leads to a unified rotationally invariant LSDA$+U$ prescription for the orbital magnetism.

Table I presents the calculated magnetic moments in UFe_2 using the LSDA$+U$. We used a generalization of the LSDA$+U$ method which takes into account that in the presence of spin-orbit coupling the occupation matrix of localized electrons becomes nondiagonal in spin indexes.[62] The matrix elements of this method contain both $F^0=U$, which provides the splitting of the localized states into "lower and upper Hubbard subbands," and the terms proportional to Slater integrals F^2, F^4, and F^6, which are responsible for angular correlations within the localized shell. In the case when U is effectively screened and $U_{\rm eff}=U-J$ becomes small, the latter terms give the dominant contribution to the corresponding matrix elements. In our LSDA$+U$ calculations we used two sets of parameters: $U=2.0$ eV and $J=0.5$ eV and $U=J=0.5$ eV. In the latter case $U_{\rm eff}=0$ and the effect of the LSDA$+U$ comes from nonspherical terms which are determined by F^2, F^4, and F^6 Slater integrals. In the following we will refer to calculations performed using the LSDA$+U$ method with $U_{\rm eff}=0$ as the LSDA$+U$(OP) calculations.

The LSDA$+U$(OP) calculations lead to almost complete cancellation of the spin and orbital magnetic moments at the U site in agreement with the experimental data. At the same time the LSDA$+U$(OP) theory still strongly overestimates the absolute value of both the spin and orbital magnetic moments at the U site in UFe_2. The total moment per formula unit becomes $1.59\mu_B$, which is larger than the LSDA computed total moment of $1.22\mu_B$ and the experimental value of $1.19\mu_B$.[11]

The LSDA$+U$ method with $U=2.0$ eV and $J=0.5$ eV strongly overestimates the spin and orbital magnetic moments at both the U and Fe sites and does not lead to the the cancellation of the spin and orbital magnetic moments at U site (Table I). One can conclude that the on-site Coulomb repulsion on the U site is suppressed, most likely because of the strong hybridization between U $5f$ and Fe $3d$ states. As a consequence, U $5f$ electrons in UFe_2 demonstrate almost purely itinerant behavior.

B. MO spectra

Another stringent test for the applicability of the itinerant LSDA approach to UFe_2 would be the description of the MO Kerr spectrum. The complex MO Kerr effect and optical reflectivity were studied experimentally in UFe_2 over the 0.6–5.0 eV energy range in Ref. 19.

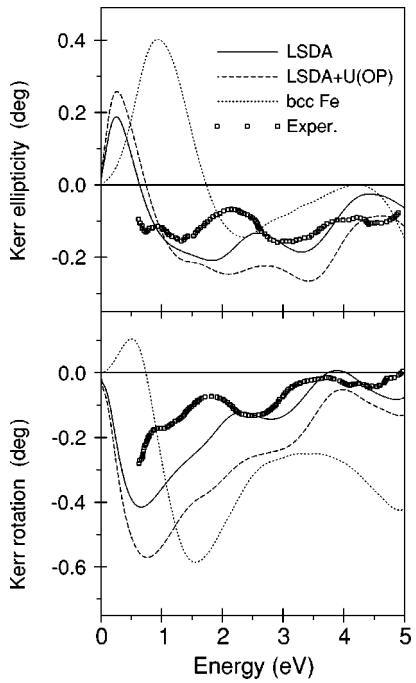

FIG. 2. Calculated and experimental Kerr rotation θ_K and Kerr ellipticity ε_K spectra of UFe_2 in comparison with the experimental data in Ref. 19 and bcc Fe.[78]

In Fig. 2 we show the calculated and experimental MO Kerr spectra of UFe_2. The Kerr spectra of UFe_2 are significantly different from the spectra of pure bcc Fe. This difference arises predominantly from substantial reduction of the magnetic moment, higher population of $3d$ states and different location of the Fermi energy E_F in UFe_2 compared to bcc Fe. The agreement between the experimental Kerr spectra of UFe_2 and the *ab initio* LSDA calculated one is rather good with the exception of a small blue shift of about 0.3 eV of the theoretically calculated prominent peak both in the Kerr rotation and ellipticity. The prominent peak at 0.6 eV in the Kerr rotation results from a combination of a deep resonance structure in the denominator $D(\omega)$ (Eq. 3) and interband transitions contributing into σ_{2xy}. Away from the peak, for energies above 1.0 eV, the Kerr rotation and ellipticity spectra are fully determined by the shape of σ_{2xy}. The LSDA$+U$(OP) approximation produces a slightly larger Kerr rotation spectrum in the whole energy interval in comparison with the LSDA calculations and the experiment. This might be connected with the overestimation of the U orbital magnetic moment in the LSDA$+U$(OP) calculations (Table I).

C. XMCD spectra

Figure 3 shows the calculated fully relativistic spin-polarized partial $5f$ density of states of ferromagnetic UFe_2. Because of the strong spin-orbit interaction of $5f$ electrons, $j=5/2$ and $j=7/2$ states are well separated in energy and the occupied states are composed mostly of $5f_{5/2}$ states whereas

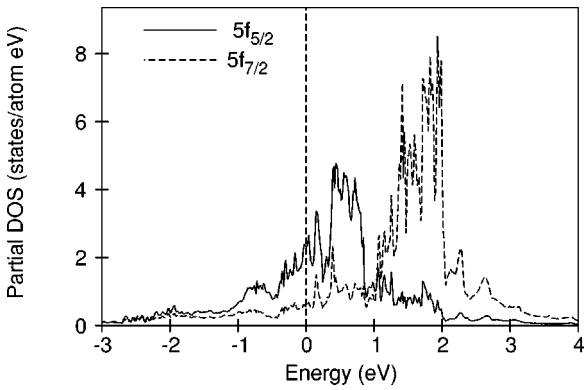

FIG. 3. The LSDA partial $5f_{5/2}$ and $5f_{7/2}$ density of states [in states/(atom eV)] in UFe_2.

$5f_{7/2}$ states are almost empty. One can note, however, that an indirect hybridization between $j=5/2$ and $j=7/2$ states via Fe $3d$ states is rather strong.

In order to compare relative amplitudes of the M_4 and M_5 XMCD spectra we first normalize the corresponding isotropic x-ray-absorption spectra (XAS) to the experimental ones taking into account the background scattering intensity as described in Sec. II. Figure 4 shows the calculated isotropic x-ray absorption and XMCD spectra in the LSDA and LSDA+U(OP) approximations together with the experimental data.[12] The contribution from the background scattering is shown by dashed lines in the upper panel of Fig. 4.

The experimentally measured dichroic M_4 line consists of a simple nearly symmetric negative peak that has no distinct structure. Such a peak is characteristic of the M_4 edge of all

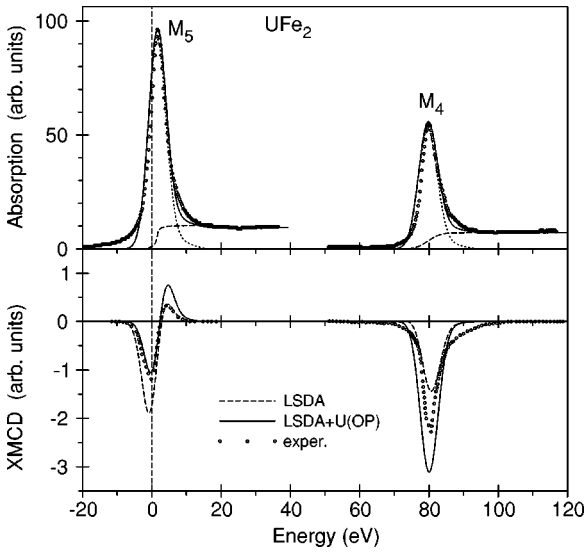

FIG. 4. Isotropic absorption and XMCD spectra of UFe_2 at the uranium $M_{4,5}$ edges calculated in the LSDA (solid lines) and LSDA+U(OP) (dashed lines) approximations. Experimental spectra[12] (circles) were measured at 20 K and at magnetic field 2 T (the U M_4 spectrum is shifted by -95 eV to include it in the figure). Upper panel also shows the background spectra (dashed line) due to the transitions from inner $3d_{3/2,5/2}$ levels to the continuum of unoccupied levels.

TABLE II. The dipole allowed transitions from core $3d_{3/2,5/2}$ levels to the unoccupied $5f_{5/2,7/2}$ valence states for left ($\lambda=+1$) and right ($\lambda=-1$) polarized x rays.

Edge	$\lambda=+1$	$\lambda=-1$
M_5	$-5/2\rightarrow-3/2$	$-5/2\rightarrow-7/2$
	$-3/2\rightarrow-1/2$	$-3/2\rightarrow-5/2$
	$-1/2\rightarrow+1/2$	$-1/2\rightarrow-3/2$
	$+1/2\rightarrow+3/2$	$+1/2\rightarrow-1/2$
	$+3/2\rightarrow+5/2$	$+3/2\rightarrow+1/2$
	$+5/2\rightarrow+7/2$	$+5/2\rightarrow+3/2$
M_4	$-3/2\rightarrow-1/2$	$-3/2\rightarrow-5/2$
	$-1/2\rightarrow+1/2$	$-1/2\rightarrow-3/2$
	$+1/2\rightarrow+3/2$	$+1/2\rightarrow-1/2$
	$+3/2\rightarrow+5/2$	$+3/2\rightarrow+1/2$

uranium systems. The dichroic line at the M_5 edge has an asymmetric s shape with two peaks—a stronger negative peak and a weaker positive peak. The dichroism at the M_4 edge is more than two times larger than at the M_5 one.

We recall that the M_4 (M_5) edge corresponds to $3d_{3/2}(3d_{5/2})\rightarrow 5f$ transitions. The created $3d$ core hole has electrostatic interaction with the $5f$ shell. However, in a first approximation, this interaction can be neglected since no clear multiplet structure is distinguished in the absorption spectra. This approximation is supported theoretically since the Slater integrals $F_k(3d,5f)$ and $G_k(3d,5f)$ are small compared to the $F_k(5f,5f)$ integrals and $3d$ spin-orbit interaction.[21] Neglecting the core-level splitting the measured spectra reflect the density of states above the Fermi level weighted by the dipole transition probabilities. Since the XMCD technique uses circular polarized x-rays, the dichroism contains information about the character of the magnetic sublevels in the DOS.

Because of the electric dipole selection rules ($\Delta l=\pm 1$; $\Delta j=0,\pm 1$) the major contribution to the absorption at the M_4 edge stems from the transitions $3d_{3/2}\rightarrow 5f_{5/2}$ and that at the M_5 edge originates primarily from $3d_{5/2}\rightarrow 5f_{7/2}$ transitions, with a weaker contribution from $3d_{5/2}\rightarrow 5f_{5/2}$ transitions. For the latter case the corresponding $3d_{5/2}\rightarrow 5f_{5/2}$ radial matrix elements are only slightly smaller than for the $3d_{5/2}\rightarrow 5f_{7/2}$ transitions. The angular matrix elements, however, strongly suppress the $3d_{5/2}\rightarrow 5f_{5/2}$ contribution. Therefore the contribution to XMCD spectrum at the M_5 edge from the transitions with $\Delta j=0$ is about 15 times smaller than the transitions with $\Delta j=1$ (see Eq. 6).

The selection rules for the magnetic quantum number m_j (m_j is restricted to $-j,\ldots,+j$) are $\Delta m_j=+1$ for $\lambda=+1$ and $\Delta m_j=-1$ for $\lambda=-1$. Table II presents the dipole allowed transitions for x-ray-absorption spectra at the M_5 and M_4 edges for left ($\lambda=+1$) and right ($\lambda=-1$) polarized x rays.

To go further, we need to discuss the characteristics of the $5f$ empty DOS. Since l and s prefer to couple antiparallel for less than half-filled shells, the $j=l-s=5/2$ has a lower energy than the $j=l+s=7/2$ level. Due to the intra-atomic exchange interaction the lowest sublevel of the $j=5/2$ will

be $m_{5/2}=-5/2$, however, for the $j=7/2$ the lowest sublevel will be $m_{7/2}=+7/2$. This reversal in the energy sequence arises from the gain in energy due to alignment of the spin with the exchange field.[25]

The $5f_{7/2}$ states are almost completely empty in all the uranium compounds. Therefore all the transitions listed in Table II are active in the M_5 absorption spectrum. The contribution from the first four transitions for $\lambda=+1$ cancels to a large extent with the contribution of the opposite sign from the last four transitions for $\lambda=-1$ having the same final states. Thus the XMCD spectrum of U at the M_5 edge ($I=\mu^- - \mu^+$) can be roughly approximated by the following sum of m_j-projected partial densities of states: $(N^{7/2}_{-7/2}+N^{7/2}_{-5/2})-(N^{7/2}_{7/2}+N^{7/2}_{5/2})$. Here we use the notation $N^j_{m_j}$ for the density of states with the total momentum j and its projection m_j. As a result, the shape of the M_5 XMCD spectrum contains two peaks of opposite signs—a negative peak at lower energy and a positive peak at higher energy. As the separation of the peaks is smaller than the typical lifetime broadening, the peaks cancel each other to a large extent, thus leading to a rather small signal. Since the splitting of states with $m_j=\pm|m_j|$ increases with the increase of the magnetization at the U site, the amplitude of the M_5 spectrum should be proportional to the U magnetic moment.

A rather different situation occurs in the case of the M_4 x-ray-absorption spectrum. Usually in uranium compounds the U atom is in $5f^3$ (U^{+3}) or $5f^2$ (U^{+4}) configurations and has partly occupied $5f_{5/2}$ states. In the first case the $5f_{5/2}$ states with $m_j=-5/2$, $-3/2$, and $-1/2$ are usually occupied. The dipole allowed transitions for $\lambda=+1$ are $-1/2\rightarrow+1/2$, $+1/2\rightarrow+3/2$, and $+3/2\rightarrow+5/2$ and those for $\lambda=-1$ are $+3/2\rightarrow+1/2$. The transitions with the same final states $m_j=+1/2$ mostly cancel each other and the XMCD spectrum of U at the M_4 edge can be roughly represented by the sum $-(N^{5/2}_{3/2}+N^{5/2}_{5/2})$. The corresponding analysis for the $5f^2$ (U^{+4}) configuration with occupied $f_{5/2,-5/2}$ and $f_{5/2,-3/2}$ states shows that the dipole allowed transitions for $\lambda=+1$ are $-3/2\rightarrow-1/2$, $-1/2\rightarrow+1/2$, $+1/2\rightarrow+3/2$, and $+3/2\rightarrow+5/2$ and for $\lambda=-1$: $+1/2\rightarrow-1/2$ and $+3/2\rightarrow+1/2$. Again, the XMCD spectrum of U at the M_4 edge can be approximated by $-(N^{5/2}_{3/2}+N^{5/2}_{5/2})$. This explains why the dichroic M_4 line in uranium compounds consists of a single nearly symmetric negative peak.

We should note, however, that the explanation of the XMCD line shape in terms of m_j-projected DOS presented above should be considered as only qualitative. First, there is no full compensation between transitions with equal final states due to difference in the angular matrix elements; second, in our consideration we neglect cross terms in the transition matrix elements; third, there is no pure $5f^3$ or $5f^2$ configurations in uranium compounds. It is always difficult to estimate an appropriate atomic $5f$ occupation number in band-structure calculations. Such a determination is usually obtained by the integration of the $5f$ electron charge density inside of the corresponding atomic sphere. In the particular UFe_2 case, the occupation number of U $5f$ states is around 2.9 in the LSDA calculations. We, however, should keep in mind that some amount of the $5f$ states are derived from the so-called ''tails'' of Fe $3d$ states arising as a result of the decomposition of the wave function centered at Fe atoms. The careful analysis in the case of UPd_3 presented in Ref. 62 shows that the occupation number of the ''tails'' of Pd $4d$ states sum up to give the $5f$ occupation of 0.9 electrons in the U atomic sphere. We should also note that due to the strong hybridization between U $5f$ and Fe $3d$ states, the U $5f_{7/2}$ states in UFe_2 are not completely empty, some of them are occupied, also some amount of U $5f_{5/2}$ states, which we have been considering as fully occupied, are partially empty.

The overall shapes of the calculated and experimental uranium $M_{4,5}$ XMCD spectra correspond well with each other (Fig. 4). The major discrepancy between the calculated and experimental XMCD spectra is the size of the M_4 XMCD peak. The LSDA underestimates the integral intensity of the XMCD at M_4 edge. As the integrated XMCD signal is proportional to the orbital moment[66] this discrepancy may be related to an underestimation of the orbital moment by LSDA-based computational methods (Table I). On the other hand, the LSDA$+U$(OP) approximation gives larger intensity for the M_4 XMCD spectrum in comparison with the experimentally measured one. It reflects the overestimation of the orbital moment at U site in the LSDA$+U$(OP) calculations (Table I). In the case of the M_5 XMCD spectrum, the LSDA reproduces the amplitude of the positive peak and overestimates the amplitude of the negative peak. The LSDA$+U$(OP) approximation, in contrast, gives good agreement in the amplitude of the negative peak but overestimates that of the positive peak.

To investigate the influence of the initial state on the resulting U XMCD spectra we calculated also the XAS and XMCD spectra of UFe_2 compound at the $N_{4,5}$ and $O_{4,5}$ edges (not shown). We found a substantial decrease of the XMCD in terms of $R=\Delta\mu/(2\mu^0)$ at $N_{4,5}$ edges in comparison with the $M_{4,5}$ ones. The theoretically calculated dichroic N_4 line consists of a simple nearly symmetric negative peak that has no distinct structure as was observed at the M_4 XMCD spectrum. The LSDA calculations give much smaller dichroic signal at the N_4 edge in comparison with the LSDA $+U(OP)$ calculations. The dichroic line at the N_5 edge is reminiscent of the corresponding M_5 spectrum and has an asymmetric *s* shape with two peaks–a stronger negative peak and much weaker positive peak. In contrast to the dichroism at the $M_{4,5}$ edges where XMCD at the M_4 edge is more than two times larger than at the M_5 one, the dichroism at the N_4 edge has almost the same intensity as at the N_5 edge.

Due to MO selection rules the O_4 XMCD spectrum resembles the M_4 spectrum, whereas the O_5 spectrum is similar to the M_5 one. Because of the relatively small spin-orbit splitting of the $5d$ states of U ($\sim$11 eV), the O_4 and O_5 spectra almost overlap each other. The magnetic dichroism at quasicore $O_{4,5}$ edges is of one order of magnitude larger than the dichroism at the $N_{4,5}$ edges and become almost as large as that at the $M_{4,5}$ edge. Besides, the lifetime broadening of the core $O_{4,5}$ levels is much smaller than the broadening of the $M_{4,5}$ ones.[79] Therefore the spectroscopy of U atoms in the ultrasoft x-ray energy range at the $O_{4,5}$ edges may be a very useful tool for investigation of the $5f$ electronic states in magnetic U materials.

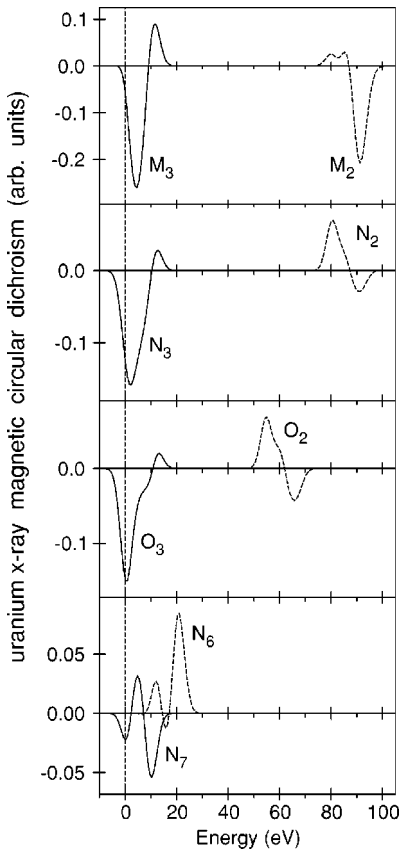

FIG. 5. XMCD spectra of UFe_2 at the uranium $M_{2,3}$, $N_{2,3}$, $O_{2,3}$, and $N_{6,7}$ edges calculated in the LSDA approximation. All the XMCD spectra are multiplied by a factor 10^2. (The M_2 and N_2 spectra are shifted by -800 eV and -150 eV, respectively, to include them in the figure).

The XAS spectra at the $M_{4,5}$, $N_{4,5}$, and $O_{4,5}$ edges involve electronic transitions between $nd_{3/2,5/2}$ ($n=3,4$, and 5) and $5f_{5/2,7/2}$ states and therefore are used to study of the $5f$ empty electronic states in uranium compounds. To investigate the $6d$ states of U one should tune the energy of the x ray close to the $M_{2,3}$, $N_{2,3}$, $O_{2,3}$, or $N_{6,7}$ edges of uranium. The first three doublets are due to the $np_{1/2,3/2} \rightarrow 6d_{3/2,5/2}$ ($n=3,4$, and 5) interband transitions.

Figure 5 presents the theoretically calculated XMCD spectra of U $M_{2,3}$, $N_{2,3}$, and $O_{2,3}$ edges. The XMCD signals at these edges are two orders of magnitude less than the corresponding signals at the $M_{4,5}$ edges.

Because of the dipole selection rules, apart from the $ns_{1/2}$-states (which have a small contribution to the XAS due to relatively small $np \rightarrow 7s$ matrix elements only $6d_{3/2}$ states occur as final states for the M_2, N_2, and O_2 XAS for unpolarized radiation, whereas for the M_3, N_3, and O_3 XAS the $6d_{5/2}$ states also contribute. Although the $np_{3/2} \rightarrow 6d_{3/2}$ radial matrix elements are only slightly smaller than for the $np_{3/2} \rightarrow 6d_{5/2}$ transitions the angular matrix elements strongly suppress the $np_{3/2} \rightarrow 6d_{3/2}$ contribution (see Eq. 6). Therefore, neglecting the energy dependence of the radial matrix elements, the M_2, N_2, and O_2 absorption spectra can be viewed as a direct mapping of the DOS curve for $6d_{3/2}$, and the M_3, N_3, and O_3 XAS reflect the DOS curve for $6d_{5/2}$ states. The shape of X_3 ($X=M,N$, or O) XMCD spectra consists of two peaks of opposite sign—a negative peak at lower energy and a positive peak at higher energy. The shape of X_2 ($X=M,N$, or O) XMCD spectra also have two peaks of an opposite sign, but the negative peaks situated at higher energy and the positive peak at lower energy (Fig. 5).

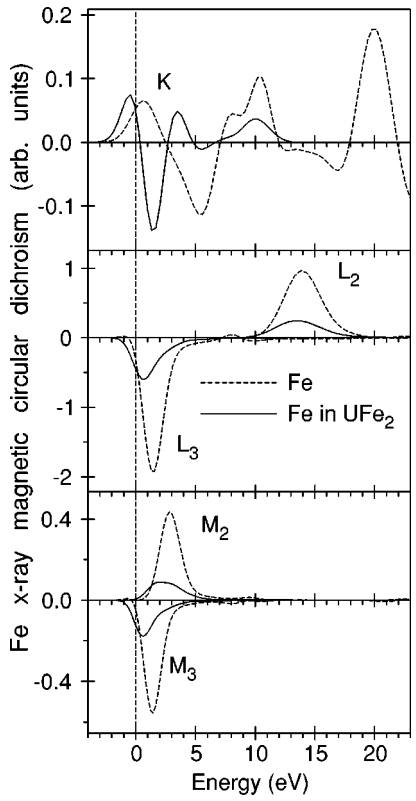

FIG. 6. XMCD spectra of UFe_2 at the Fe K, $L_{2,3}$, and $M_{2,3}$ edges in bcc Fe and Fe in UFe_2 calculated in the LSDA approximation. The XMCD spectrum at the K edge has been multiplied by a factor 10^2.

Figure 5 also presents the theoretically calculated XMCD spectra at U $N_{6,7}$ edges. Because of the electric dipole selection rules the major contribution to the absorption at the N_7 edge stems from the transitions $4f_{7/2} \rightarrow 6d_{5/2}$ and that at the N_6 edge originates primarily from $4f_{5/2} \rightarrow 6d_{3/2}$ transitions (the contribution from $4f_{5/2} \rightarrow 6d_{5/2}$ transitions are strongly suppressed by the angular matrix elements). The XMCD signals at these edges are even smaller than the corresponding signals at the $X_{2,3}$ ($X=M,N$, or O) edges. Because of the relatively small spin-orbit splitting of the $4f$ states of U, the N_6 and N_7 spectra have an appreciable overlap. Besides, in the case of $N_{6,7}$ XAS one would expect a strong electrostatic interaction between the created $4f$ core hole and the valence states. It can lead to an additional multiplet structure in the XAS and XMCD spectra at the $N_{6,7}$ edges. We have not considered multiplet structure in our XMCD calculations. This structure can be captured using full atomic multiplet structure calculations.

We also calculated the x-ray magnetic circular dichroism at the Fe K, $L_{2,3}$, and $M_{2,3}$ edges, with the results being presented in Fig. 6. For comparison we also show the XMCD spectra in bcc Fe. Although the XMCD signal at the

Fe K edge has almost the same amplitude both in bcc Fe and UFe_2, their shapes are quite different (Fig. 6). Because dipole allowed transitions dominate the absorption spectrum for unpolarized radiation, the absorption coefficient $\mu_K^0(E)$ (not shown) reflects primarily the DOS of unoccupied $4p$-like states $N_p(E)$ of Fe above the Fermi level. Due to the energy dependent radial matrix element for the $1s \rightarrow 4p$ there is no strict one-to-one correspondence between $\mu_K(E)$ and $N_p(E)$. The exchange splitting of the initial $1s$ core state is extremely small,[80] therefore only the exchange and spin-orbit splitting of the final $4p$ states is responsible for the observed dichroism at the K edge. For this reason the dichroism is found to be very small (Fig. 6). It was first pointed out by Gotsis and Strange[81] as well as Brooks and Johansson[82] that XMCD K-spectrum reflects the orbital polarization in differential form $d\langle l_z \rangle / dE$ of the p states. It gives a rather simple and straightforward interpretation of the Fe XMCD spectrum at the K edge.[55]

In contrast to the K edge, the dichroism at Fe L_2 and L_3 edges is also influenced by the spin-orbit coupling of the initial $2p$ core states. This gives rise to a very pronounced dichroism in comparison with the dichroism at the K edge. Figure 6 shows the theoretically calculated Fe $L_{2,3}$ XMCD spectra in UFe_2 and bcc Fe. The dichroism at the L_3 edge has a negative sign and at the L_2 edge a positive one. The XMCD dichroic signals at the Fe $L_{2,3}$ and $M_{2,3}$ edges are three times smaller in UFe_2 than the corresponding XMCD in bcc Fe due to strongly reduced magnetic moment at the Fe site in UFe_2 in comparison with pure Fe. Besides, the shape of the spectra is more asymmetrical in UFe_2.

The magnetic dichroism at the Fe $M_{2,3}$ edges is much smaller than at the $L_{2,3}$ edges (Fig. 6). Besides the M_2 and the M_3 spectra are strongly overlapped and the M_3 spectrum contributes to some extent to the structure of the total $M_{2,3}$ spectrum in the region of the M_2 edge. To decompose a corresponding experimental $M_{2,3}$ spectrum into its M_2 and M_3 parts will therefore be quite difficult in general. It is worth mentioning that the shape of Fe L_3 and M_3 XMCD spectra are very similar.

IV. SUMMARY

We have studied by means of an *ab initio* fully relativistic spin-polarized Dirac linear muffin-tin orbital method the electronic structure, magneto-optical properties, and the x-ray magnetic circular dichroism in UFe_2.

Polarized neutrons and elastic scattering[10,11] as well as x-ray magnetic circular dichroism measurements[12] reveal that the orbital and spin magnetic moments on the U site are almost equal and oppositely directed, hence the U net moment, which is the sum of the orbital and spin contributions, is close to zero in UFe_2. The LSDA calculations do not provide such a compensation. On the other hand, a generalization of the LSDA+U method (with $U_{\text{eff}}=0$, the LSDA +U(OP) approximation) leads to almost complete cancellation of the spin and orbital magnetic moments at the U site, in good agreement with neutron and XMCD experimental data. However the LSDA+U(OP) theory still strongly overestimates the absolute value of both the spin and orbital magnetic moments at the U site in UFe_2.

The agreement between the experimental Kerr spectra and the *ab initio* LSDA calculated ones is rather good. The prominent peak in the Kerr rotation at around 0.6 eV results from the interplay of a deep resonance structure in the denominator and interband transitions contributing to σ_{2xy}. Away from the peak, for energies above 1.0 eV, the Kerr rotation and ellipticity spectra are fully determined by the shape of σ_{2xy}. The LSDA+U(OP) approximation produces a larger Kerr rotation spectrum in the whole energy interval in comparison with the LSDA calculations and the experiment. It might be connected with the overestimation of the U orbital magnetic moment in the LSDA+U(OP) calculations. These findings illustrate that not everything about the electronic structure of UFe_2 is explained.

The experimentally measured dichroic M_4 line consists of a simple nearly symmetric negative peak that has no distinct structure. The dichroic line at the M_5 edge has an asymmetric s shape with two peaks—a stronger negative peak and a weaker positive peak. The overall shapes of the calculated and experimental uranium $M_{4,5}$ XMCD spectra correspond well with each other. The major discrepancy between the calculated and experimental XMCD spectra is in the amplitude of the M_4 XMCD peak. The LSDA underestimates the integral intensity of the XMCD at M_4 edge. As the integrated XMCD signal is proportional to the orbital moment this discrepancy may be related to the underestimation of the orbital moment by LSDA-based computational methods. On the other hand, the LSDA+U(OP) approximation gives larger intensity for the M_4 XMCD spectrum in comparison with the experimentally measured one. It reflects the overestimation of the orbital moment at U site in the LSDA+U(OP) calculations. In the case of the M_5 XMCD spectrum, the LSDA produces a correct value of the positive peak and overestimates the value of the negative peak. The LSDA+U(OP) approximation, in contrast, gives good agreement in the value for the negative peak and overestimates the positive peak.

The line shape of the dichroic spectra can be qualitatively understood considering the MO selection rules as well as the occupation and the energy sequence of the m_j-projected partial densities of states. The $5f_{7/2}$ states are almost completely empty in all the uranium compounds and the XMCD spectrum of U at the M_5 edge can be roughly approximated by the following sum of partial densities of $5f_{7/2}$ states: $(N^{7/2}_{-7/2}+N^{7/2}_{-5/2})-(N^{7/2}_{7/2}+N^{7/2}_{5/2})$. As a result, the shape of the M_5 XMCD spectrum stems from two peaks of opposite signs—a negative peak at lower energy and a positive peak at higher energy. As the separation of the peaks is smaller than the typical lifetime broadening, the peaks cancel each other to a large extent, thus leading to a rather small signal.

A rather different situation occurs in the case of the M_4 x-ray-absorption spectrum. Uranium compounds have partially occupied $5f_{5/2}$ states and the XMCD spectrum of U at the M_4 edge can be approximated by $-(N^{5/2}_{3/2}+N^{5/2}_{5/2})$. This explains why the dichroic M_4 line in uranium compounds consists of a single nearly symmetric negative peak.

The XMCD signals at U $M_{2,3}$, $N_{2,3}$, $O_{2,3}$, and $N_{6,7}$ edges are two orders of magnitude weaker than the corresponding signals at the $M_{4,5}$ edges.

Due to small exchange splitting of the initial $1s$ core states only the exchange and spin-orbit splitting of the final $4p$ states are responsible for the observed dichroism at Fe K edge. The XMCD spectra of Fe for the $L_{2,3}$ edge are mostly determined by the strength of the SO coupling of the initial $2p$ core states and spin-polarization of the final empty $3d_{3/2,5/2}$ states while the exchange splitting of the $2p$ core states as well as the SO coupling of the $3d$ valence states are of minor importance.

ACKNOWLEDGMENTS

This work was carried out at the Ames Laboratory, which is operated for the U.S. Department of Energy by Iowa State University under Contract No. W-7405-82. This work was supported by the Office of Basic Energy Sciences of the U.S. Department of Energy. V.N. Antonov gratefully acknowledges the hospitality at Ames Laboratory during his stay.

*Email address: antonov@ameslab. gov; anton@imp.kiev.ua; Permanent address: Institute of Metal Physics, Vernadsky Street, 03142 Kiev, Ukraine.

[1] A.T. Aldred, J. Magn. Magn. Mater. **10**, 42 (1979).
[2] A.V. Andreev, A.V. Deryagin, R.Z. Levitin, A.S. Markosyan, and M. Zeleny, Phys. Status Solidi A **52**, K13 (1979).
[3] Y.F. Popov, R.Z. Levitin, M. Zaleny, A.V. Deryagin, and A.V. Andreev, Sov. Phys. JETP **51**, 1223 (1980).
[4] K.P. Belov, G.I. Kataev, R.Z. Levin, S.A. Nikitin, and V.I. Sokolov, Sov. Phys. Usp. **26**, 518 (1983).
[5] T.P. Sorokina, G.M. Kvashnin, and A.M. Kapitonov, Phys. Met. Metallogr. **66**, 164 (1988).
[6] V.V. Eremenko, N.E. Kamer, and V.D. Chercherskii, Sov. Phys. JETP **67**, 241 (1988).
[7] M. Yessik, J. Appl. Phys. **40**, 1133 (1969).
[8] G.H. Lnder, A.T. Aldred, B.D. Dunlap, and G.K. Shenoy, Physica B **86-88**, 152 (1977).
[9] M.S.S. Brooks, O. Eriksson, B. Johansson, J.J.M. Franse, and P.H. Frings, J. Phys. F: Met. Phys. **18**, L33 (1988).
[10] M. Wulff, G.H. Lander, B. Lebech, and A. Delapalme, Phys. Rev. B **39**, 4719 (1989).
[11] B.L.M. Wulff, G.H. Lander, J. Rebizant, J.C. Spirlet, and A. Delapalme, J. Phys.: Condens. Matter **1**, 10 299 (1989).
[12] M. Finazzi, P. Sainctavit, A.M. Dias, J.P. Kappler, G. Krill, J.P. Sanchez, P.D. de Reotier, A. Yaouanc, A. Rogalev, and J. Goulon, Phys. Rev. B **55**, 3010 (1997).
[13] P.K. Lawson, M.J. Cooper, M.A.G. Dixon, D.N. Timms, E. Zukowski, F. Itoh, and H. Sakurai, Phys. Rev. B **56**, 3239 (1997).
[14] J. Ghisen, R.L. Johnson, J.C. Spirtel, and J.J.M. Franse, J. Electron Spectrosc. Relat. Phenom. **37**, 163 (1985).
[15] J. Ghisen, J. Electron Spectrosc. Relat. Phenom. **35**, 19 (1985).
[16] L. Paolasini, G.H. Lander, S.M. Shapiro, R. Caciuffo, B. Lebech, L.P. Regnault, B. Roessli, and J.M. Fournier, Phys. Rev. B **54**, 7222 (1996).
[17] L. Paolasini, R. Caciuffo, B. Roessli, G.H. Lander, K. Myers, and P. Canfield, Phys. Rev. B **59**, 6867 (1999).
[18] L. Paolasini, B. Hennion, A. Panchula, K. Myers, and P. Canfield, Phys. Rev. B **58**, 12 125 (1998).
[19] M. Kucera, P. Berankova, and I. Tichy, J. Magn. Magn. Mater. **196-197**, 604 (1999).
[20] P.M. Oppeneer, A.Y. Perlov, V.N. Antonov, A.N. Yaresko, T. Kraft, and M.S. Brooks, J. Alloys Compd. **271-273**, 831 (1998).
[21] S.P. Collins, D. Laundy, C.C. Tang, and G. van der Laan, J. Phys.: Condens. Matter **7**, 9325 (1995).
[22] N. Kernavanois, P.D. de Reotier, A. Yaouanc, J.P. Sanchez, V. Honkimäki, T. Tschentscher, J. McCarthy, and O. Vogt, J. Phys.: Condens. Matter **13**, 9677 (2001).
[23] P.D. de Reotier, J.P. Sanchez, A. Yaouanc, M. Finazzi, P. Sainctavit, G. Krill, J.P. Kappler, J. Goedkoop, J. Goulon, C. Goulon-Ginet, A. Rogalev, and O. Vogt, J. Phys.: Condens. Matter **9**, 3291 (1997).
[24] A. Bombardi, N. Kernovanois, P.D. de Reotier, G.H. Lander, J.P. Sanchez, A. Yaouanc, P. Burlet, E. Lelievre-Berna, A. Rogalev, O. Vogt, and K. Mattenberger, Eur. Phys. J. B **21**, 547 (2001).
[25] P.D. de Reotier, A. Yaouanc, G. van der Laan, N. Kernavanois, J.P. Sanchez, J.L. Smith, A. Hiess, A. Huxley, and A. Rogalev, Phys. Rev. B **60**, 10 606 (1999).
[26] P.D. de Reotier, J.P. Sanches, and A. Yaouanc, J. Alloys Compd. **271-273**, 414 (1998).
[27] N. Kernavanois, J.X. Boucherle, P.D. de Reotier, F. Givord, E. Lelievre-Berna, E. Ressouche, A. Rogalev, J.P. Sanchez, N. Sato, and A. Yaouanc, J. Phys.: Condens. Matter **12**, 7857 (2000).
[28] A. Yaouanc, P.D. de Reotier, G. van der Laan, A. Hiess, J. Goulon, C. Neumann, P. Lejay, and N. Sato, Phys. Rev. B **58**, 8793 (1998).
[29] W. Grange, M. Finazzi, J.P. Kappler, A. Dellobe, G. Krill, P. Sainctavit, J.P. Sanchez, A. Rogalev, and J. Goulon, J. Alloys Compd. **275-277**, 583 (1998).
[30] M. Kucera, J. Kunes, A. Kolomiets, M. Divis, A.V. Andreev, V. Sechovsky, J.P. Kappler, and A. Rogalev, Phys. Rev. B **66**, 144405 (2002).
[31] H. Ebert, Rep. Prog. Phys. **59**, 1665 (1996).
[32] J.P. Hannon, G.T. Trammell, M. Blume, and D. Gibbs, Phys. Rev. Lett. **61**, 1245 (1988).
[33] S.W. Lovsey and S.P. Collins, *X-Ray Scattering and Absorption in Magnetic Materials* (Oxford University Press, Oxford, 1996).
[34] J.B. Kortright and S.-K. Kim, Phys. Rev. B **62**, 12 216 (2000).
[35] W. Reim and J. Schoenes, in *Ferromagnetic Materials*, edited by E.P. Wohlfarth and K.H.J. Buschow (North-Holland, Amsterdam, 1990), Vol. 5, p.133.
[36] W.H. Kleiner, Phys. Rev. **142**, 318 (1966).
[37] F.U. Hillebrecht, C. Roth, H.B. Rose, W.G. Park, E. Kisker, and Phys. Rev. B **55**, 2594 (1997).
[38] J.G. Menchero, Phys. Rev. B **57**, 993 (1998).
[39] G. van der Laan, J. Magn. Magn. Mater. **148**, 53 (1995).
[40] G. van der Laan, J. Electron Spectrosc. Relat. Phenom. **86**, 41 (1997).
[41] G. van der Laan, J. Phys.: Condens. Matter **9**, L259 (1997).
[42] G. van der Laan, Phys. Rev. B **57**, 5250 (1998).
[43] J.G. Menchero, Phys. Rev. B **57**, 1001 (1998).
[44] A. Fanelsa, R. Schellenberg, F.U. Hillebrecht, E. Kisker, J.G.

Menchero, A.P. Kaduwela, C.S. Fadley, and M.A.V. Hove, Phys. Rev. B **54**, 17 962 (1996).
[45] J.G. Menchero, C.S. Fadley, G. Panaccione, F. Sirotti, G.J. Henk, and R. Feder, Phys. Rev. B **55**, 11 476 (1997).
[46] J.G. Menchero, Phys. Rev. B **55**, 5505 (1997).
[47] R. Schellenberg, E. Kisker, A. Fanelsa, F.U. Hillebrecht, J.G. Menchero, A.P. Kaduwela, C.S. Fadley, and M.A.V. Hove, Phys. Rev. B **57**, 14 310 (1998).
[48] H. Ebert, L. Baumgarten, C.M. Schneider, and J. Kirschner, Phys. Rev. B **44**, 4406 (1991).
[49] H. Ebert and G.-Y. Guo, J. Magn. Magn. Mater. **148**, 178 (1995).
[50] G.Y. Guo, H. Ebert, W.M. Temmerman, and P.J. Durham, Phys. Rev. B **50**, 3861 (1994).
[51] E. Tamura, G.D. Waddill, J.G. Tobin, and P.A. Sterne, Phys. Rev. Lett. **73**, 1533 (1994).
[52] V.V. Nemoshkalenko, V.N. Antonov, V.N. Antonov, W. John, H. Wonn, and P. Ziesche, Phys. Status Solidi B **111**, 11 (1982).
[53] F.K. Richtmyer, S.W. Barnes, and E. Ramberg, Phys. Rev. **46**, 843 (1934).
[54] V.N. Antonov, B.N. Harmon, A.N. Yaresko, and A.Y. Perlov, Phys. Rev. B **59**, 14 571 (1999).
[55] V.N. Antonov, B.N. Harmon, and A.N. Yaresko, Phys. Rev. B **63**, 205112 (2001).
[56] O.K. Andersen, Phys. Rev. B **12**, 3060 (1975).
[57] V.V. Nemoshkalenko, A.E. Krasovskii, V.N. Antonov, V.N. Antonov, U. Fleck, H. Wonn, and P. Ziesche, Phys. Status Solidi B **120**, 283 (1983).
[58] U. von Barth and L. Hedin, J. Phys. C **5**, 1629 (1972).
[59] P.E. Blöchl, O. Jepsen, and O.K. Andersen, Phys. Rev. B **49**, 16 223 (1994).
[60] V.N. Antonov, A.I. Bagljuk, A.Y. Perlov, V.V. Nemoshkalenko, V.N. Antonov, O.K. Andersen, and O. Jepsen, Low Temp. Phys. **19**, 494 (1993).
[61] V.I. Anisimov, J. Zaanen, and O.K. Andersen, Phys. Rev. B **44**, 943 (1991).
[62] A.N. Yaresko, V.N. Antonov, and P. Fulde, Phys. Rev. B **67**, 155103 (2003).
[63] G.G. Scott, J. Phys. Soc. Jpn. **17**, 372 (1962).
[64] W. Marshall and S.W. Lovsey, *Theory of Thermal Neutron Scattering* (Oxford University Press, Oxford, 1971).
[65] M. Blume, J. Appl. Phys. **57**, 3615 (1985).
[66] B.T. Thole, P. Carra, F. Sette, and G. van der Laan, Phys. Rev. Lett. **68**, 1943 (1992).
[67] P. Carra, B.T. Thole, M. Altarelli, and X. Wang, Phys. Rev. Lett. **70**, 694 (1993).
[68] M.S.S. Brooks and B. Johansson, in *Handbook of Magnetic Materials*, edited by K.H.J. Buschow (North-Holland, Amsterdam, 1993), Vol. 7, p. 139.
[69] M.S.S. Brooks, Physica B **130**, 6 (1985).
[70] O. Eriksson, M.S.S. Brooks, and B. Johansson, Phys. Rev. B **41**, 7311 (1990).
[71] L. Severin, M.S.S. Brooks, and B. Johansson, Phys. Rev. Lett. **71**, 3214 (1993).
[72] A. Mavromaras, L. Sandratskii, and J. Kübler, Solid State Commun. **106**, 115 (1998).
[73] G. Vignale and M. Rasolt, Phys. Rev. Lett. **59**, 2360 (1987).
[74] P. Skudlarski and G. Vignale, Phys. Rev. B **48**, 8547 (1993).
[75] M. Higuchi and A. Haegawa, J. Phys. Soc. Jpn. **66**, 149 (1997).
[76] S.V. Beiden, W.M. Temmerman, Z. Szotek, and G.A. Gehring, Phys. Rev. Lett. **79**, 4970 (1997).
[77] I.V. Solovyev, A.I. Liechtenstein, and K. Terakura, Phys. Rev. Lett. **80**, 5758 (1998).
[78] V.N. Antonov, A.Y. Perlov, A.P. Shpak, and A.N. Yaresko, J. Magn. Magn. Mater. **146**, 205 (1995).
[79] J.C. Fuggle and J.E. Inglesfield, *Unoccupied Electronic States*, Topics in Applied Physics, Vol. 69 (Springer, New York, 1992).
[80] H. Ebert, J. Phys.: Condens. Matter **1**, 9111 (1989).
[81] H.J. Gotsis and P. Strange, J. Phys.: Condens. Matter **6**, 1409 (1994).
[82] M.S.S. Brooks and B. Johansson, in *Spin-Orbit Influenced Spectroscopies*, edited by H. Ebert and G. Schütz (Springer, Berlin, 1996), p. 211.